

## Homoatomic Stella Quadrangula $[\text{Ti}_8]^{6-}$ in $\text{Cs}_{18}\text{Ti}_8\text{O}_6$ , Interplay of Spin–Orbit Coupling, and Jahn–Teller Distortion

Ulrich Wedig, Vyacheslav Saltykov, Jürgen Nuss, and Martin Jansen\*

Max Planck Institute for Solid State Research, Heisenbergstr. 1, 70569 Stuttgart, Germany

Received June 11, 2010; E-mail: M.Jansen@fkf.mpg.de

**Abstract:**  $\text{Cs}_{18}\text{Ti}_8\text{O}_6$  was synthesized reacting the binary compounds  $\text{CsTi}$  and  $\text{Cs}_2\text{O}$ . According to single crystal X-ray analysis, the title compound crystallizes as a novel structure type in the cubic space group  $I23$  and is diamagnetic. The electronic structure of the extended solid and of excised  $\text{Cs}_6\text{Ti}_8$  clusters has been examined by relativistic density functional calculations including spin–orbit coupling.  $\text{Cs}_{18}\text{Ti}_8\text{O}_6$  comprises a clusteranion  $[\text{Ti}_8]^{6-}$  in the shape of a tetrahedral star. An isoelectronic cluster was found previously in  $\text{Cs}_8\text{Ti}_8\text{O}$ , however, with the shape of a parallelepiped. Both clusteranions can be derived from a homocubane unit by displacive distortions. It has been shown by quantum mechanical analyses that the closed-shell electronic structure of the parallelepiped is the result of a Jahn–Teller distortion, while in contrast the tetrahedral star in  $\text{Cs}_{18}\text{Ti}_8\text{O}_6$  would still exhibit an open-shell degenerate HOMO within a scalar relativistic approximation. Only if spin–orbit coupling is considered, a closed-shell electronic system is obtained in accordance with the diamagnetic behavior of  $\text{Cs}_{18}\text{Ti}_8\text{O}_6$ .

### Introduction

The contraction of the electronic shell of the atoms with growing nuclear charge is one of the basic factors causing the periodicity in the properties of chemical elements. Evidently, this effect, and its consequences for the electronic structure of an atom, is most substantial for heavy atoms having nuclear charges higher than  $\sim 50$ , where the speeds at which the electrons move in the vicinity of the nuclei are approaching the velocity of light. At least starting at this point, it is indispensable to consider the relativistic dependence of the electron mass on its speed, in the context of electronic structure calculations. The differences resulting between nonrelativistic and relativistic quantum mechanical treatments have been denoted as “relativistic effects”,<sup>1</sup> distinguishing direct (contraction and stabilization of  $s$  and  $p$  shells, spin–orbit coupling) and indirect (expansion and destabilization of  $d$  and  $f$  shells) effects. Experimentally, significant respective peculiarities in the chemical and physical properties of heavy elements have indeed been identified. The most pronounced pertinent features occur with gold and platinum,<sup>1</sup> which can both exist as monovalent and divalent anions, respectively, in fully charge ordered bulk solids.<sup>2</sup> Furthermore, gold as an anion has been demonstrated to have a rich and diverse chemistry.<sup>1f</sup> It widely resembles the halogens, in that elemental gold disproportionates

in an alkaline environment<sup>3</sup> and  $\text{Au}^-$  can function as an acceptor in hydrogen bonds<sup>4</sup> and displays a crystal chemistry quite analogous to halides.<sup>5</sup> However, these conspicuous experimental findings cannot be straightforwardly attributed to “relativistic effects”, since gold and platinum are unique in that they are the first elements that have experienced the  $d$  and  $f$  contractions in an immediate sequence. Thus, conventional orbital and relativistic effects are superimposed.<sup>6</sup>

Spin–orbit coupling and its enhancement with growing nuclear charge is of relativistic origin exclusively,<sup>7</sup> in contrast to the orbital contraction and expansion effects. Due to strong relativistic spin–orbit coupling, the degeneracy of the Russell–Saunders ground state of a  $6p^2$  configuration is lifted and a diamagnetic ground state  $(6p_{1/2}^2)_0$  results. The concomitant lowering in energy is e.g. reflected by the first ionization potential of lead exceeding the one of bismuth, which has a half filled  $p$ -shell. For all corresponding pairs of lighter elements the reverse sequence in ionization potentials is observed. We regard  $\text{Ti}^-$  as a candidate to express a closed shell  $(6p_{1/2}^2)_0$  configuration in a solid state compound. For example a still hypothetical solid like  $\text{Cs}_3\text{TlO}$  being diamagnetic could only be

- (1) (a) Desclaux, J.-P. *At. Data Nucl. Data Tables* **1973**, *12*, 311–406. (b) Pyykkö, P. *Chem. Rev.* **1988**, *88*, 563–594. (c) Schwerdtfeger, P., Ed. *Relativistic Electronic Structure Theory*; Elsevier Science B.V.: Amsterdam, The Netherlands, 2002. (d) Hess, B. A., Ed. *Relativistic Effects in Heavy-Element Chemistry and Physics*; John Wiley & Sons: New York, 2003. (e) Jansen, M. *Solid State Sci.* **2005**, *7*, 1464–1474. (f) Jansen, M. *Chem. Soc. Rev.* **2008**, *37*, 1824–1835.
- (2) (a) Peer, W. J.; Lagowski, J. J. *J. Am. Chem. Soc.* **1978**, *100*, 6260–6261. (b) Hensel, F. Z. *Phys. Chem.* **1980**, *154*, 201–219. (c) Feldmann, C.; Jansen, M. *Angew. Chem.* **1993**, *105*, 1107–1108; *Angew. Chem., Int. Ed. Engl.* **1993**, *32*, 1049–1050. (d) Karpov, A.; Nuss, J.; Wedig, U.; Jansen, M. *Angew. Chem.* **2003**, *115*, 4966–4969; *Angew. Chem., Int. Ed.* **2003**, *42*, 4818–4821.

- (3) (a) Mudring, A.-V.; Nuss, J.; Wedig, U.; Jansen, M. *J. Solid State Chem.* **2000**, *155*, 29–36. (b) Mudring, A.-V.; Jansen, M. *Angew. Chem.* **2000**, *112*, 3194–3196; *Angew. Chem., Int. Ed.* **2000**, *39*, 3066–3067. (c) Nuss, J.; Jansen, M. *Z. Anorg. Allg. Chem.* **2009**, *635*, 1514–1516.
- (4) Nuss, H.; Jansen, M. *Angew. Chem.* **2006**, *118*, 4476–4479; *Angew. Chem., Int. Ed.* **2006**, *45*, 4369–4371.
- (5) (a) Feldmann, C.; Jansen, M. *Z. Anorg. Allg. Chem.* **1995**, *621*, 1907–1912. (b) Nuss, J.; Jansen, M. *Z. Kristallogr. New Cryst. Struct.* **2002**, *217*, 313.
- (6) (a) Seth, M.; Dolg, M.; Fulde, P.; Schwerdtfeger, P. *J. Am. Chem. Soc.* **1995**, *117*, 6597–6598. (b) Autschbach, J.; Siekierski, S.; Seth, M.; Schwerdtfeger, P.; Schwarz, W. H. E. *J. Comput. Chem.* **2002**, *23*, 804–813.
- (7) (a) Dirac, P. A. M. *Proc. R. Soc. London, Ser. A* **1928**, *117*, 610–624. (b) Dirac, P. A. M. *Proc. R. Soc. London, Ser. A* **1928**, *118*, 351–361.

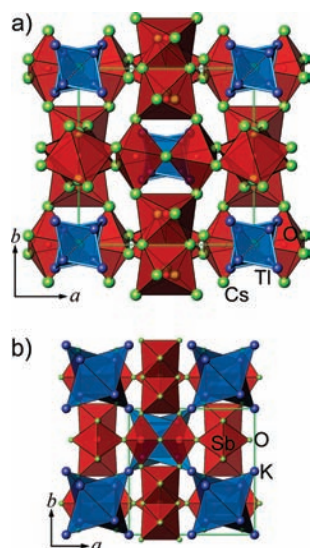


**Figure 1.** Graphical presentation of the crystal structure of Cs<sub>18</sub>Tl<sub>8</sub>O<sub>6</sub> (a) (Tl<sub>8</sub> clusters emphasized as blue polyhedra; OCs<sub>6</sub> octahedra in red) and of K<sub>8</sub>SbO<sub>6</sub> (b) (SbO<sub>6</sub> octahedra in red; the K atoms are depicted as a corner-connected array of K<sub>8</sub> stellae quadrangulae). Green lines mark the unit cell edges.

understood in terms of relativistic quantum mechanics. With the objective of realizing solids containing isolated Tl<sup>−</sup> anions, we have started to investigate the systems Rb/Tl/O and Cs/Tl/O. A number of compounds featuring novel and interesting structural properties have been obtained from these combinations of elements;<sup>8</sup> however, no evidence for the existence of “isolated” thallium(−I) was gained. Instead, in each case thallium cluster ions were identified, corroborating the well-known propensity of thallium in negative oxidation states to form homoatomic clusters.<sup>9,10</sup> Here we report on Cs<sub>18</sub>Tl<sub>8</sub>O<sub>6</sub> (Figure 1a) containing a homocubane-like clusteranion with the shape of a double tetrahedron (*stella quadrangula*<sup>11</sup> or tetrahedral star), not found before in compounds containing covalently bonded homoatomic clusters. An isoelectronic clusteranion was detected previously in Cs<sub>8</sub>Tl<sub>8</sub>O,<sup>8a</sup> however, with the different shape of a parallelepiped. Both clusters can be derived from an ideal cube by displacive distortions. In order to investigate the mechanisms leading to the two different shapes, scalar and fully relativistic density functional calculations including spin–orbit coupling have been performed, opposing

Jahn–Teller distortion and spin–orbit coupling as two competing mechanisms to obtain a closed-shell electronic system.

## Experimental Method

Because both, educts and products, are very sensitive to air and moisture, all operations were performed under dried argon (Schlenk technique or glovebox with H<sub>2</sub>O, O<sub>2</sub> < 0.1 ppm; MB 150B-G-II, M. Braun GmbH, München, Germany). Cs<sub>18</sub>Tl<sub>8</sub>O<sub>6</sub> was prepared by reaction of the binary compounds CsTl and Cs<sub>2</sub>O. Cesium thallide was produced by reaction of cesium (synthesized from CsCl by reduction with Ca and distilled twice in vacuum)<sup>12</sup> with thallium (ChemPur, Jülich, 99.999%, dried before use at 393 K in dynamic vacuum at 10<sup>−3</sup> mbar during 12 h) in the molar ratio 2:1 (total amount: 2–3 g) in a tantalum tube which was sealed under argon with an arc-welder. The reaction mixture was heated with a rate of 50 K/h up to 773 K, annealed at this temperature for 2 days, and then cooled to room temperature with a rate of 5 K/h. The excess of cesium was distilled off at 373 K in a dynamic vacuum of 10<sup>−3</sup> mbar. Cesium oxide was synthesized from Cs by oxidation with a slight deficiency of oxygen followed by distillation of the excess Cs.<sup>12</sup> The mixture of CsTl and Cs<sub>2</sub>O in the molar ratio 1:1 (total amount 0.5–1 g) was placed into a tantalum tube following the packing procedure described above. The reaction mixture was heated at a rate of 50 K/h up to 573 K, annealed at this temperature for 1 week, and then cooled to room temperature at a rate of 5 K/h. The as-synthesized products were pure, sometimes containing small amounts of Cs<sub>4</sub>Tl<sub>2</sub>O and Cs<sub>8</sub>Tl<sub>11</sub> (1–4 wt %), according to X-ray powder diffraction. The atom ratio of heavy elements in the product was additionally confirmed by using a scanning electron microscope (XL 30 TMP, Philips, Netherlands), equipped with an integrated EDAX-EDX system.

Single-crystal X-ray diffraction data of Cs<sub>18</sub>Tl<sub>8</sub>O<sub>6</sub> were collected using a Bruker AXS APEX-SMART-diffractometer with a graphite monochromator and corrected for absorption effects (SADABS).<sup>13</sup> The structure was solved and refined with SHELXTL.<sup>14</sup> Crystal structure data of Cs<sub>18</sub>Tl<sub>8</sub>O<sub>6</sub>:<sup>15</sup> cubic, *I*23 (no. 197), *a* = 13.3724(3) Å, *V* = 2391.27(9) Å<sup>3</sup>, ρ<sub>calcd</sub> = 5.727 g·cm<sup>−3</sup>, *Z* = 2, μ(Mo Kα) = 40.366 mm<sup>−1</sup>, *F*(000) = 3372, λ = 0.710 73 Å, *T* = 298(2) K, ω-scan, 18 656 measured reflections, 1316 symmetry independent reflections (2θ<sub>max</sub> = 69.84°), 27 refined parameters. Atom coordinates: Tl1 (8c) 0.91059(2), *x*, *x*; Tl2 (8c) 0.13439(2), *x*, *x*; Cs1 (12*d*) 0.36483(5), 0, 0; Cs2 (24*f*) 0.21363(3), 0.4483(1), 0.17401(3); O1 (12*e*) 0.3270(5), 1/2, 0; *R*<sub>1</sub> = 0.0248, *wR*<sub>2</sub> = 0.0519 (1570 *F*<sub>0</sub> > 4σ(*F*<sub>0</sub>)); *R*<sub>1</sub> = 0.0299, *wR*<sub>2</sub> = 0.0536 (all). Residual electron density: 1.253/−1.174 e·Å<sup>−3</sup>.

The thermal stability was studied using Differential Scanning Calorimetry (DSC 404 C Pegasus, Netzsch GmbH, Selb, Germany). The specimen (0.0184 g) was placed in an Al crucible with a lid, cold-sealed to prevent access of air and heated to 673 K at a rate of 2 K/min, and then cooled down to room temperature at the same rate. The whole process was run under argon. Magnetization was measured using a SQUID magnetometer (MPMS 5.5, Quantum Design, USA) in the temperature range 5–300 K at *H* = 0.001, 0.1, 1, 3, 5, and 7 T. The specimen

- (8) (a) Karpov, A.; Jansen, M. *Angew. Chem.* **2005**, *117*, 7813–7816; *Angew. Chem., Int. Ed.* **2005**, *44*, 7639–7643. (b) Karpov, A.; Jansen, M. *Chem. Commun.* **2006**, 1706–1708.
- (9) (a) Corbett, J. D. In *Structural And Electronic Paradigms In Cluster Chemistry (Structure and Bonding, Vol. 87)*; Mingos, D. M. P., Ed.; Springer-Verlag: Berlin, Germany, 1997; pp 157–193. (b) Corbett, J. D. *Angew. Chem.* **2000**, *112*, 682–704; *Angew. Chem., Int. Ed.* **2000**, *39*, 670–690.
- (10) (a) Hansen, D. A.; Smith, J. F. *Acta Crystallogr. Sect. A: Found. Crystallogr.* **1967**, *22*, 836–845. (b) Dong, Z.-C.; Corbett, J. D. *J. Am. Chem. Soc.* **1994**, *116*, 3429–3435. (c) Dong, Z.-C.; Corbett, J. D. *Angew. Chem.* **1996**, *108*, 1073–1076; *Angew. Chem., Int. Ed. Engl.* **1996**, *35*, 1006–1009. (d) Dong, Z.-C.; Corbett, J. D. *J. Am. Chem. Soc.* **1995**, *117*, 6447–6455. (e) Dong, Z.-C.; Corbett, J. D. *J. Cluster Sci.* **1995**, *6*, 187–201. (f) Huang, D. P.; Dong, Z.-C.; Corbett, J. D. *Inorg. Chem.* **1998**, *37*, 5881–5886. (g) Kaskel, S.; Corbett, J. D. *Inorg. Chem.* **2000**, *39*, 778–782. (h) Dong, Z.-C.; Corbett, J. D. *J. Am. Chem. Soc.* **1993**, *115*, 11299–11303. (i) Dong, Z.-C.; Corbett, J. D. *Inorg. Chem.* **1996**, *35*, 2301–2306.
- (11) Hyde, B. G.; Andersson, S. *Inorganic Crystal Structures*; John Wiley & Sons: New York, 1989; pp 342–344.

- (12) Brauer, G. *Handbuch der Präparativen Anorganischen Chemie*, Vol. 2; Ferdinand Enke: Stuttgart, Germany, 1978; pp 938–954.
- (13) Sheldrick, G. M. *SADABS - Bruker AXS area detector scaling and absorption*, version 2008/1; University of Göttingen: Germany, 2008.
- (14) Sheldrick, G. M. *Acta Crystallogr.* **2008**, *A64*, 112–122.
- (15) Further details of the crystal structure investigations may be obtained from the Fachinformationszentrum Karlsruhe, 76344 Eggenstein-Leopoldshafen, Germany (fax: (+49)7247-808-666; e-mail: crysdata(at)fiz-karlsruhe.de) on quoting the depository number CSD-421376.

(0.1309 g) was sealed in a quartz tube under helium. The raw data were corrected for the holder contribution.

## Theoretical Methods

DFT calculations using the PBE functional<sup>16</sup> were performed for the crystal structures as determined experimentally as well as for isolated  $\text{Cs}_6\text{Tl}_8$  clusters representing charge neutral cut-outs of the crystal. The band structures of the periodic systems were computed with the WIEN2k<sup>17</sup> code, using the following computational parameters. Radii of the atomic spheres: 2.9 bohr (Tl), 2.7 bohr (Cs), and 2.7 bohr (O); cutoff parameter  $\text{RKmax} = 7.0$ ;  $\text{Gmax} = 14.0$ . The Kohn–Sham equations were solved for 119 k-points in the irreducible wedge of the Brillouin zone. The core–valence separation was set to  $-6.0$  Ry. Thus 13 electrons of Tl, 19 electrons of Cs, and 6 electrons of O were taken as valence electrons, being treated scalar relativistic. The APW+lo basis was applied, added by local orbitals for  $l = 2$  (Tl, Cs) and  $l = 0$  (Cs, O). Spin–orbit interaction was included by a second-variational method.<sup>18</sup> The isolated  $\text{Cs}_6\text{Tl}_8$  clusters were computed with the TURBOMOLE<sup>19</sup> program package, applying the RI-variant. The def2-TZVP basis set was used. Scalar relativistic effects were included by the choice of the proper pseudopotentials: Tl, 21 valence electrons;<sup>20</sup> Cs, 9 valence electrons.<sup>21</sup> In the two-component relativistic calculations, the spin–orbit variant of the Tl pseudopotential was used. In the scalar relativistic case the structures of the clusters were optimized with ( $O_h$ ,  $T_d$ , and  $D_{3d}$ ) and without symmetry constraints. The energy was converged to  $10^{-9}$  a.u., the maximum norm of the Cartesian gradient to  $10^{-5}$  a.u. The existence of a minimum was verified by a frequency analysis. As analytical gradients are not yet available in the two component version of TURBOMOLE, the fully relativistic structure optimizations were done numerically, presuming  $O_h$ ,  $T_d$ , and  $D_{3d}$  symmetry respectively. Effective charges of the atoms in the crystals were calculated from the integrated electron densities within the atomic basins, obtained by a topological analysis of the electron density.<sup>22</sup>

## Results and Discussion

**Synthesis and Properties.**  $\text{Cs}_{18}\text{Tl}_8\text{O}_6$  was synthesized by reacting binary CsTl and  $\text{Cs}_2\text{O}$  at 573 K, followed by slow cooling to room temperature in arc-welded tantalum ampules. The product was obtained as black brittle crystals. The best results were achieved by reacting the starting materials in a molar ratio of 1:1, which implies evaporation of excess  $\text{Cs}_2\text{O}$  and Cs from the sample. The purity of the product sensitively depends on purity, handling, and composition of the starting mixtures as well as on precise control of the reaction conditions.  $\text{Cs}_{18}\text{Tl}_8\text{O}_6$  can be obtained as a single phase. The most frequently occurring admixtures (1–4 wt %) are  $\text{Cs}_4\text{Tl}_2\text{O}^{23}$  and  $\text{Cs}_8\text{Tl}_{11}$ .<sup>10e</sup>  $\text{Cs}_{18}\text{Tl}_8\text{O}_6$  is extremely sensitive to moisture and air and is stable

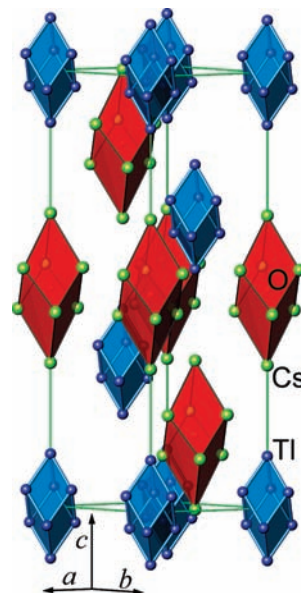


**Figure 2.** Graphical presentation of the crystal structure of  $\text{Cs}_8\text{Tl}_8\text{O}_6$ .<sup>8a</sup>  $\text{Tl}_8$  clusters emphasized as blue polyhedra;  $\text{Cs}_8$  polyhedra in red, centered by oxygen.

up to 573 K in an argon atmosphere. The magnetic susceptibility is temperature independent in the range of 50 to 300 K ( $-6.84 \times 10^{-4}$  emu/mol  $\pm$  2.5%) and approximates the sum of diamagnetic core corrections ( $18\chi(\text{Cs}^+) + 8\chi(\text{Tl}^+) + 6\chi(\text{O}^{2-}) = -9.02 \times 10^{-4}$  emu/mol) and the Larmor susceptibility<sup>24</sup> of the cluster orbital electrons ( $-1.91 \times 10^{-4}$  emu/mol), which was calculated assuming the shape of an ideal cube with a side length of 3.111 Å.

**Structure.** According to the results of an X-ray single-crystal structure analysis,  $\text{Cs}_{18}\text{Tl}_8\text{O}_6$  crystallizes in a novel structure type (Figure 1a) displaying isolated  $[\text{Tl}_8]^{6-}$  units with the shape of a tetrahedral star, a so-called *stella quadrangula*,<sup>11</sup> and is the first example of a covalently bonded, homoatomic cluster with such an arrangement. The oxygen atoms are surrounded by six cesium atoms in the shape of a distorted octahedron. The Cs–O distances of 2.936 Å ( $4\times$ ) and 2.862 Å ( $2\times$ ) comply well with those in  $\text{Cs}_2\text{O}$  (2.87 Å),<sup>25</sup> which is indicative of a full ionization of the Cs atoms. The electrons, which are released from the Cs/O partial structure, are accommodated by the isolated  $[\text{Tl}_8]^{6-}$  groups. Cesium and oxygen are constituting a three-dimensional network of corner and edge sharing octahedra  ${}^3_6[\text{OCs}_6\text{O}_2]^+$  (Figure 1a). The resulting framework is providing voids, sufficient in number and size, to accommodate the  $\text{Tl}_8$  clusters. A similar three-dimensional topology is realized in the  $\text{KSbO}_3$ <sup>26</sup> structure type (Figure 1b), where the Sb atoms are surrounded by six O atoms.

**The  $[\text{Tl}_8]^{6-}$  Clusteranion.** Interestingly, the title compound and the previously reported  $\text{Cs}_8\text{Tl}_8\text{O}_6$ <sup>8a</sup> contain  $\text{Tl}_8$ -clusters displaying the same number of valence electrons, however, of different structures, a tetrahedral star (Figure 1a) or a parallelepiped (Figure 2). Both clusters can be formally described as  $[\text{Tl}_8]^{6-}$  clusteranions having 30 valence electrons available.

(16) Perdew, J. P.; Burke, K.; Ernzerhof, M. *Phys. Rev. Lett.* **1996**, *77*, 3865–3868.

(17) Blaha, P.; Schwarz, K.; Madsen, G. K. H.; Kvasnicka, D.; Luitz, J. *WIEN2k, An Augmented Plane Waves + Local Orbitals Program for Calculating Crystal Properties*; Schwarz, K., Ed.; Techn. Universität Wien: Austria, 2001.

(18) Novák, P. [http://www.wien2k.at/reg\\_user/textbooks/novak\\_lecture\\_on\\_spinorbit.ps](http://www.wien2k.at/reg_user/textbooks/novak_lecture_on_spinorbit.ps).

(19) (a) *TURBOMOLE V6.1*, University of Karlsruhe and Forschungszentrum Karlsruhe GmbH, TURBOMOLE GmbH, <http://www.turbomole.com>, 2009. (b) Armbruster, M. K.; Weigend, F.; van Wüllen, C.; Klopper, W. *Phys. Chem. Chem. Phys.* **2008**, *10*, 1748–1756.

(20) Metz, B.; Schweizer, M.; Stoll, H.; Dolg, M.; Liu, W. *Theor. Chem. Acc.* **2000**, *104*, 22–28.

(21) Leininger, T.; Nicklass, A.; Küchle, W.; Stoll, H.; Dolg, M.; Bergner, A. *Chem. Phys. Lett.* **1996**, *255*, 274–280.

(22) Bader, R. F. W. *Atoms in Molecules: a Quantum Theory*; Oxford University Press: Oxford, 1990.

(23) Saltykov, V.; Nuss, J.; Jansen, M. Unpublished results.

(24) (a) Ashcroft, N. W.; Mermin, N. D. *Solid State Physics*; Holt, Rinehart and Winston: Philadelphia, 1976; p 649. (b) Sevov, S. C.; Corbett, J. D. *Inorg. Chem.* **1992**, *31*, 1895–1901.

(25) Tsai, K.-R.; Harris, P. M.; Lassette, E. N. *J. Phys. Chem.* **1956**, *60*, 338–344.

(26) Spiegelberg, P. *Arkiv foer Kemi, Mineralogi och Geologi* **1940**, *A14*, 1–2.

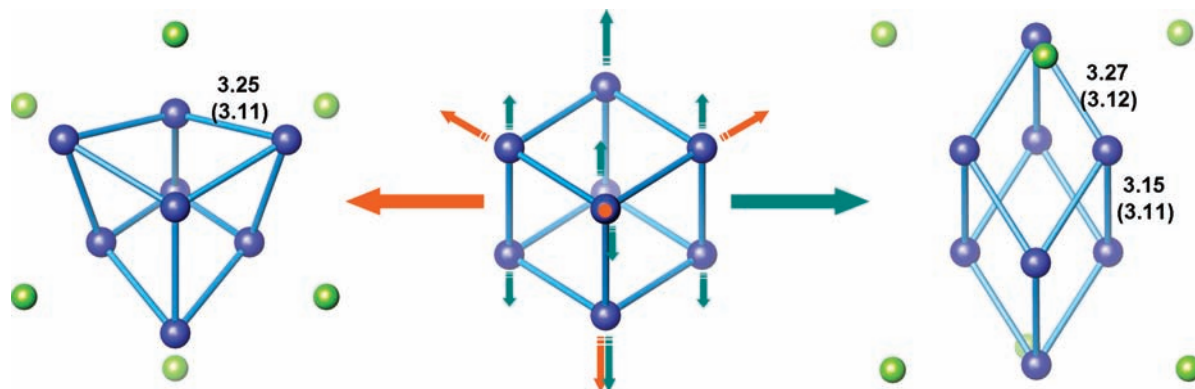


**Figure 3.** Optimized structures of  $\text{Cs}_6\text{Tl}_8$  clusters. The shapes of the  $\text{Tl}_8$  units conform to the polyhedra found in  $\text{Cs}_{18}\text{Tl}_8\text{O}_6$  (left, tetrahedral star) and in  $\text{Cs}_8\text{Tl}_8\text{O}$  (right, parallelepiped). The symmetry-unique computed (two component relativistic, PBE, def2-TZVP) Tl–Tl distances are given in Å. The corresponding experimental values found for the crystal are added in parentheses.

Neither of them can be understood in terms of known qualitative concepts. Within the Zintl–Klemm concept, which is based on  $2e2c$  bonds, the number of valence electrons should be 40 (12 edges  $\times 2e + 8$  inert pairs) for both, the tetrahedral star and the parallelepiped. Also applying Wade’s rules fails: a *closo* cluster  $[\text{Tl}_8]^{6-}$  would require  $34e$  ( $4 \times 8 + 2$ , inert-electron pairs included), which is in conflict with the  $30e$  available. The  $[\text{Tl}_8]^{6-}$  cluster can best be denoted as hypoelectronic<sup>9b</sup> with  $2n-2$  skeletal electrons ( $14e$ , disregarding  $2 \times 8e$  for the lone pairs).

**Electronic Structure Calculations.** Topologically, both  $\text{Tl}_8$  units considered can be derived from an ideal cube by a displacive distortion as sketched in Figure 3. Remarkably, in either case the lattice symmetries would allow accommodation of  $\text{Tl}_8$  units of cubic shape since the site symmetries are subgroups of  $O_h$ . Moreover, the nearest neighbors ( $\text{Cs}^+$  ions) do exert but a weak crystal field, and their positions could either be easily reconciled with a high symmetric clusteranion by slight displacive movements ( $\text{Cs}_8\text{Tl}_8\text{O}$ ) or already display the higher symmetry ( $\text{Cs}1 \times 6: O_h$ ) in comparison to the tetrahedral star ( $T_d$ ) in  $\text{Cs}_{18}\text{Tl}_8\text{O}_6$ . In order to understand the driving forces behind the distortions, and thus to resolve these puzzling inconsistencies, we have performed density functional (DFT) calculations on the periodic crystals as well as on respective isolated  $\text{Cs}_6\text{Tl}_8$  clusters for both compounds. As both clusteranions derive from a cube, a hypothetical  $\text{Cs}_{18}\text{Tl}_8\text{O}_6$  crystal with an ideal cubic  $\text{Tl}_8$  unit (side length: 3.11 Å) was also examined. All the results discussed in the following are based on the PBE<sup>16</sup> functional for exchange and correlation. Data obtained with a hybrid functional, remarks on basis set effects, and further details, especially on the scalar relativistic calculations, can be found in the Supporting Information.

The periodic DFT calculations for the  $\text{Cs}_{18}\text{Tl}_8\text{O}_6$  crystal at the scalar relativistic level result in a spin-polarized electronic system with a finite density of states (DOS) of the majority spin component at the Fermi level (Figure 4a), indicating half-metallic properties of the crystal, which is in contrast to the observed diamagnetism. This discrepancy is resolved, however, if relativistic spin–orbit coupling is included in the calculations. The spin polarization vanishes, and a gap (0.18 eV) between valence and conduction bands in the crystal opens (Figure 4b and first column in Figure 5). The band structure of  $\text{Cs}_8\text{Tl}_8\text{O}$  looks similar. However, in contrast to  $\text{Cs}_{18}\text{Tl}_8\text{O}_6$ , for this compound no spin polarization but a band gap results already at the scalar relativistic level (Figure 4e). Considering spin–orbit coupling does not change the electronic structure of  $\text{Cs}_8\text{Tl}_8\text{O}$

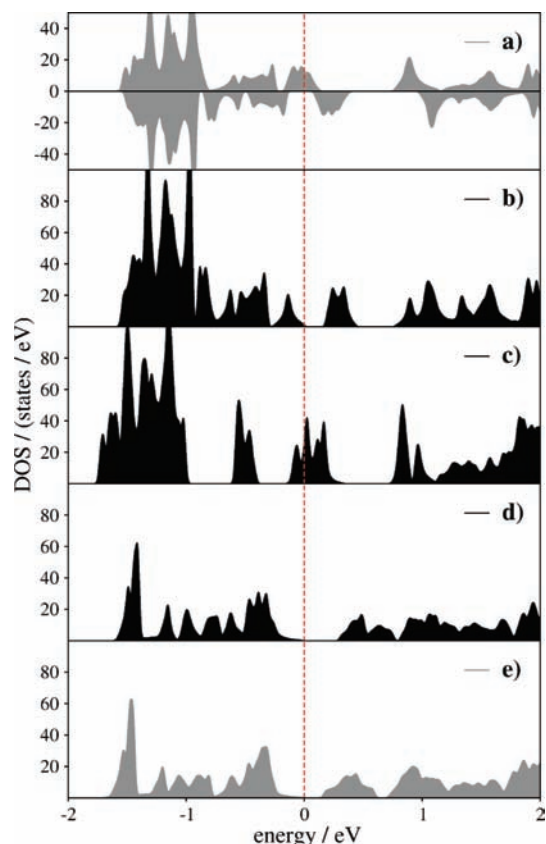


**Figure 4.** Total densities of states (DOS) near the Fermi level of  $\text{Cs}_{18}\text{Tl}_8\text{O}_6$  (a and b), hypothetical  $\text{Cs}_{18}\text{Tl}_8\text{O}_6$  with cubic  $\text{Tl}_8$  unit (c), and  $\text{Cs}_8\text{Tl}_8\text{O}$  (d and e). Gray: without spin–orbit coupling (a and e); black: including spin–orbit coupling (b, c, and d).

in principle (Figure 4d and columns 5–7 in Figure 5). Calculations on the hypothetical  $\text{Cs}_{18}\text{Tl}_8\text{O}_6$  crystal with the ideal cubic  $\text{Tl}_8$  unit yield a finite DOS at the Fermi level even with spin–orbit coupling (Figure 4c).

The analysis of the charge distribution by a topological analysis of the computed electron density<sup>22</sup> does not provide an explanation for the different shapes of the  $\text{Tl}_8$  units in either compound  $\text{Cs}_{18}\text{Tl}_8\text{O}_6$  or  $\text{Cs}_8\text{Tl}_8\text{O}$ . The effective charges are quite similar ( $\text{Cs}_{18}\text{Tl}_8\text{O}_6$ : Tl1  $-0.44$ , Tl2  $-0.49$ , Cs1  $+0.68$ , Cs2  $+0.67$ , O  $-1.40$ ;  $\text{Cs}_8\text{Tl}_8\text{O}$ : Tl1  $-0.46$ , Tl2  $-0.50$ , Cs1  $+0.65$ , Cs2  $+0.64$ , O  $-1.39$ ), revealing a charge transfer of comparable size to the  $\text{Tl}_8$  unit ( $\text{Cs}_{18}\text{Tl}_8\text{O}_6$ :  $-3.68$ ;  $\text{Cs}_8\text{Tl}_8\text{O}$ :  $-3.78$ ).

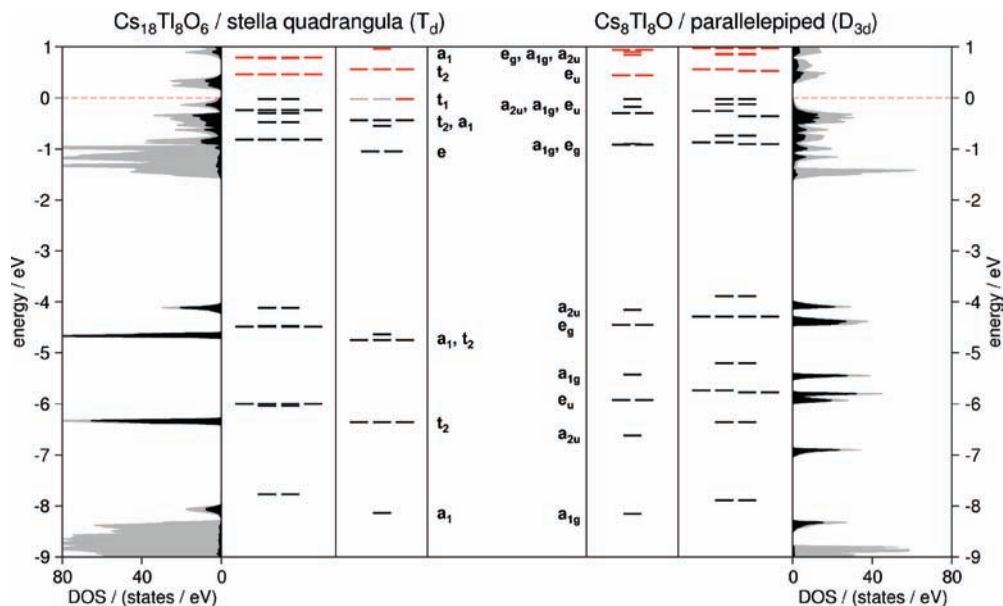


**Figure 5.** Density of states (DOS) of the crystals and MO diagrams of the  $\text{Cs}_6\text{Tl}_8$  clusters. Left side:  $\text{Cs}_{18}\text{Tl}_8\text{O}_6$  and tetrahedral star; right side:  $\text{Cs}_8\text{Tl}_8\text{O}$  and parallelepiped. The diagrams show scalar relativistic MOs (majority spin, column 3 and 5; occupied: black; partially occupied: gray; unoccupied: red), fully relativistic spinors (column 2 and 6), and DOS including spin–orbit coupling (column 1 and 7; total DOS: gray; TI-projected DOS: black).  $E_F$  and  $\epsilon_{\text{HOMO}}$  are shifted to 0 eV.

Effective charges derived from quantum chemical calculations suffer in some respect from arbitrariness.<sup>27</sup> Nevertheless, as effective charges tend to be lower than formal charges,<sup>28</sup> the high cumulative negative charge in the  $\text{Tl}_8$  units justifies their formal description as  $[\text{Tl}_8]^{6-}$ . Moreover, it suggests discussion of the peculiarities of the clusteranions in a local picture, comparing the electronic structures obtained on the various types of excised, charge neutral  $\text{Cs}_6\text{Tl}_8$  molecular units (clusters) with those calculated for the extended solids.

The results for the molecular units are based on optimized structures. When spin–orbit coupling is neglected, the lowest minimum found on the potential energy surface with no symmetry restrictions corresponds to a  $\text{Tl}_8$  unit with the shape of a parallelepiped with  $D_{3d}$  symmetry (Figure 3, right side), comparable to the  $\text{Tl}_8$  unit found experimentally in  $\text{Cs}_8\text{Tl}_8\text{O}$ . The Cs atoms take roughly the positions of Cs1 in the crystal. This minimum is a closed-shell singlet state. If the symmetry is constrained to  $T_d$ , which is the symmetry of the tetrahedral star in  $\text{Cs}_{18}\text{Tl}_8\text{O}_6$ , the minimum corresponds to an open-shell triplet state which is 13 kJ/mol lower than an open-shell singlet of same symmetry. But even the triplet state is less stable by 24 kJ/mol than the parallelepiped. If, however, fully relativistic calculations including spin–orbit coupling are performed, both the parallelepiped and the tetrahedral star configuration are closed-shell systems and, moreover, the energetic order of both configurations is reversed: The tetrahedral star is now 13 kJ/mol more stable than the parallelepiped. Thus the contribution of spin–orbit coupling to the stabilization of the tetrahedral star amounts to 37 kJ/mol. The optimized Tl–Tl distances in both configurations are represented in Figure 3, together with the corresponding distances measured in the crystals. If the symmetry is constrained to  $O_h$ , forcing a cubic arrangement of the Tl atoms, the cluster remains an open-shell system ( $\langle S_z \rangle = 0.54$ ) even with spin–orbit coupling. Such a cluster with an ideal

$\text{Tl}_8$ -cube is 79 kJ/mol less stable than the tetrahedral star. It will be worthwhile to analyze the ratio of electrostatic and relativistic forces contributing to the Jahn–Teller coupling of this cubic cluster according to the procedure as described in ref 29 for tetrahedral systems. This will be subject to future investigations.

For comparison of the DOS of the extended structures with the MO diagrams calculated for the isolated cluster types (Figure 5), the atom-projected DOS of the oxygen atoms (at  $-1$  to  $-2$  eV) can be disregarded. The spatial separation and the shielding by the Cs atoms render any covalent interaction with the clusteranions insignificant. Besides the O-projected DOS, only contributions of the interstitial space and of the Tl atoms are found at energies above  $-8.2$  eV. The latter are highlighted in Figure 5. The cluster MOs map very well onto the TI-projected DOS in both cases,  $\text{Cs}_{18}\text{Tl}_8\text{O}_6$  and  $\text{Cs}_8\text{Tl}_8\text{O}$ . The respective partial DOS in the valence region split into two parts. Below  $-4$  eV, eight very narrow, partially degenerate bands appear per  $\text{Tl}_8$  unit, which correspond to the lower MOs of the cluster in the same energy region. This part of the electronic structure can be attributed to the inert-electron pairs of the Tl atoms. The marginal dispersion of these bands points to a high localization. In the nonrelativistic limit, the corresponding energy levels are shifted upward by more than 1 eV, indicating that these bands are stabilized significantly by scalar relativistic effects. The bands between  $-1$  eV and  $E_F$  (set to 0 eV) correspond to the 14 skeletal electrons of the  $n$ -atomic cluster ( $2n-2$ ). The pronounced similarity of the MO patterns of the  $\text{Cs}_6\text{Tl}_8$  clusters and the densities of states of the extended crystals as well as the analogies concerning the open- and closed-shell electronic structures support the view of covalently bonded clusteranions.

The ideal cubic arrangement leads to an open shell system at any level of theory applied in this work. Its stretching along the body diagonal leading to the parallelepiped in  $\text{Cs}_8\text{Tl}_8\text{O}$  can be regarded as a Jahn–Teller distortion, resulting in a closed-

(27) Jansen, M.; Wedig, U. *Angew. Chem.* **2008**, *120*, 10176–10180; *Angew. Chem., Int.* **2008**, *47*, 10026–10029.

(28) Meister, J.; Schwarz, W. H. E. *J. Phys. Chem.* **1994**, *98*, 8245–8252.

(29) Opalka, D.; Segado, M.; Poluyanov, L. V.; Domcke, W. *Phys. Rev. A* **2010**, *81*, 042501.

shell electronic system. In  $\text{Cs}_{18}\text{Tl}_8\text{O}_6$  the situation is more complicated. The tetrahedral star results from moving the two subsets of each of the four tetrahedrally arranged Tl atoms constituting the cube inward and outward, respectively, and still maintains a high symmetry ( $T_d$ ). In a scalar relativistic MO picture, such an arrangement cannot be understood in terms of the Jahn–Teller theorem, as in this case the compound would still take a spin-polarized, open-shell electronic structure. Only in a fully relativistic treatment, which includes spin–orbit coupling, the tetrahedral star becomes a closed-shell electronic system, in accordance with the experimental findings. At this level of theory, the tetrahedral star can be regarded as a Jahn–Teller distorted cube. The stabilization of the cluster anion due to spin–orbit interaction has turned out to be much larger for the tetrahedral star than for the parallelepiped. Thus both shapes of  $[\text{Tl}_8]^{6-}$  become competitive local minima on the potential energy surface, and both shapes are realized in compounds of the Cs/Tl/O system, depending on the ratio of the three constituents.

## Conclusions

Following a fundamental principle in chemistry, given configurations tend to stabilize by opening a gap between the highest occupied and the lowest unoccupied electronic states. As a special manifestation of this principle, highly symmetric species with degenerate frontier orbitals stabilize by geometric distortion, thus lifting electronic degeneracy and arriving at a closed-shell system (Jahn–Teller or Peierls distortion). In the cluster chemistry of heavy main group elements, spin–orbit coupling is an alternative mechanism leading to a nondegenerate HOMO. Here, we present the first experimental evidence for such a mechanism that was previously disclosed theoretically e.g. for Pb clusters.<sup>19b</sup> Quantum chemical calculations, both for the extended solid and for excised, charge neutral molecular units, clearly show that a closed-shell electronic system in accordance with the magnetic properties is achieved for the highly symmetric tetrahedral star in  $\text{Cs}_{18}\text{Tl}_8\text{O}_6$  only if spin–orbit coupling is taken into account.

Moreover, spin–orbit interaction not only influences the electronic state but also changes the relative energies of various cluster configurations. For the  $[\text{Tl}_8]^{6-}$  cluster contained in

$\text{Cs}_8\text{Tl}_8\text{O}$ , which has the same number of (valence) electrons but a different structure compared to the one in  $\text{Cs}_{18}\text{Tl}_8\text{O}_6$ , the correct structure is already reproduced on the scalar relativistic level. Since a regular cube  $[\text{Tl}_8]^{6-}$  would display an open-shell degenerate ground state, the distortion encountered in  $\text{Cs}_8\text{Tl}_8\text{O}$  can be completely understood in terms of the Jahn–Teller theorem. Spin–orbit coupling does not yield in a qualitatively different ground state, but results in a destabilization relative to the tetrahedral star, thus making both cluster configurations competitive. The discrimination between the kind of cluster realized depends on the boundary conditions imposed on the overall structures of the hosting extended solids. The higher content of  $\text{Cs}_2\text{O}$  in  $\text{Cs}_{18}\text{Tl}_8\text{O}_6 = \text{Cs}_6\text{Tl}_8 \cdot 6\text{Cs}_2\text{O}$  as compared to  $\text{Cs}_8\text{Tl}_8\text{O} = \text{Cs}_6\text{Tl}_8 \cdot \text{Cs}_2\text{O}$  alone already enforces substantially different crystal structures.

Furthermore, our analyses revealed traditional approaches admissible to qualitatively addressing the causal relationship between electron counts and structures of clusters, which like e.g. the Zintl–Klemm concept or Wade’s rules are based on considering isolated clusters, excised from the solid. Our treatments regarding the  $[\text{Tl}_8]^{6-}$  clusters embedded in the solid or as charge neutral  $\text{Cs}_6\text{Tl}_8$  units have rendered rather consistent results. In light of the new insights provided, it appears worthwhile to revisit the extended family of homoatomic thallium cluster ions, which have so far been eluding a coherent and conclusive interpretation of their electronic structures, in striking contrast to boron based clusters to which the classical rules nicely apply.

**Acknowledgment.** The authors thank E. Brücher for performing the magnetic measurements.

**Supporting Information Available:** Crystallographic information file (CIF); checkCIF report; coordinates file of various structures of  $\text{Cs}_6\text{Tl}_8$ ; further DOS diagrams; additional computational results concerning the molecular units, basis sets, and functionals. This material is available free of charge via the Internet at <http://pubs.acs.org>.

JA1051022